SU-SEL-65-096

The Bistatic Continuous-Wave Radar Method for the Study of Planetary Surfaces

by

G. L. Tyler

October 1965

Scientific Report No. 13

Prepared under

National Aeronautics and Space Administration

Research Grant NsG-377

RADIOSCIENCE LABORATORY

STANFORD ELECTRONICS LABORATORIES

STANFORD UNIVERSITY • STANFORD, CALIFORNIA

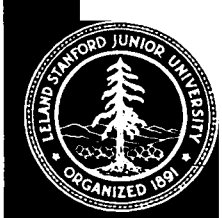

SEL-65-096

THE BISTATIC CONTINUOUS-WAVE RADAR METHOD FOR THE STUDY OF PLANETARY SURFACES

by

G. L. Tyler

October 1965

Scientific Report No. 13

Prepared under
National Astronautics and Space Administration
Grant NsG-377

Radioscience Laboratory
Stanford Electronics Laboratories
Stanford University Stanford, California

ABSTRACT

12967

A method is proposed for obtaining radar maps of the surface of a planet. This method is based on the use of a bistatic, continuous-wave mode of radar operation between the Earth and a spacecraft orbiting the planet. If the planet is illuminated by radio transmission from the Earth, and if the orbiter samples both the illuminating wave and the wave scattered by the planet, the amplitude and phase of the scattered wave may be recovered by a comparison of the two. This information may then be processed to create a focused image of the original brightness distribution, and resolution of a few wavelengths in range and azimuth can theoretically be obtained. Evaluation of the technique indicates that it is feasible to apply it to Mars, Venus, and the Moon. Author

LIST OF ILLUSTRATIONS

NOTATION

a	extremities of path
b	
c	speed of light
e_i	incident field
e_s	scattered field
f	ratio of path length to range
g	current distribution
j	$\sqrt{-1}$
$\bar{k}$	wave vector
p	spatial dispersion factor
$\bar{r}$	position vector
t	time
u_{max}	greatest frequency in e_s
v	volume
A	a constant
B	isolated spherical body
C	Fresnel integral for cosine
E	total energy of the signal
I	intensity of response
L	satellite trajectory
N_o	spectral density of noise
P	power
S	Fresnel integral for sine

NOTATION (Continued)

λ	wavelength of radiation fields
θ	apparent angle between a line to L and the plane containing g
ξ	direction cosine
ω	radian frequency
$*$	convolution (as $g*p$)
$*$	complex conjugate (as e_i^*)

ACKNOWLEDGMENT

I gratefully acknowledge the assistance of J. W. Goodman and D. W. Jackson of the Stanford Systems Techniques Laboratory for performing the experimental work presented in Figs. 7 through 9, and of my research advisor, V. R. Eshleman.

This report presents a novel method for obtaining radar maps--i.e., radar brightness distributions--of other planets and the Moon--by employing a bistatic, continuous-wave mode of radar operation between an orbiting space vehicle and an Earth station. The technique is a simple extension of "wavefront reconstruction" introduced by Gabor [Ref. 1] for microscopy except that now an orbiter is used to sample the radio-frequency interference pattern formed by an illuminating wave and the fields scattered by a planet. In the case of high signal-to-noise ratios these maps will have a resolution of a few to a few-hundred wavelengths; for very low signal-to-noise ratios resolutions of several thousand wavelengths can be achieved. Such maps will provide detailed information on the structure and composition of planetary surfaces--information that has not previously been obtained and that cannot be obtained by optical observations alone. In the case of Venus, radar maps would apparently provide one of the few means, other than direct exploration, for studying the surface.

For the purpose of constructing a model, consider an isolated spherical body B, which for the moment is assumed to be stationary. Let the body B be illuminated by a monochromatic radio source on the Earth, which is sufficiently removed from B for the incident fields e_i, to be considered plane. Call the fields scattered by the body e_s. B is also assumed to be much much larger than the wavelength of the illumination and to possess a surface that is smooth on the scale of its size even though it may deviate many wavelengths from its mean. The Moon, Mars, and Venus satisfy these conditions except for the stationarity assumption. Further assume that B is encircled by an orbiting spacecraft that samples the fields along its orbit. To simplify matters somewhat, let the spacecraft be equipped with an antenna that views B on only one side of its ground track. Over a short portion of its orbit the vehicle's trajectory is approximately linear. It therefore seems reasonable to adopt the following model for bistatic-radar mapping.

In the coordinate system of Fig. 1 let the straight line from (x_o, a, z_o) to (x_o, b, z_o) represent the satellite trajectory. (This straight-line assumption will be removed later.) Denote this line by L. Considering each vector component of the fields separately and using complex

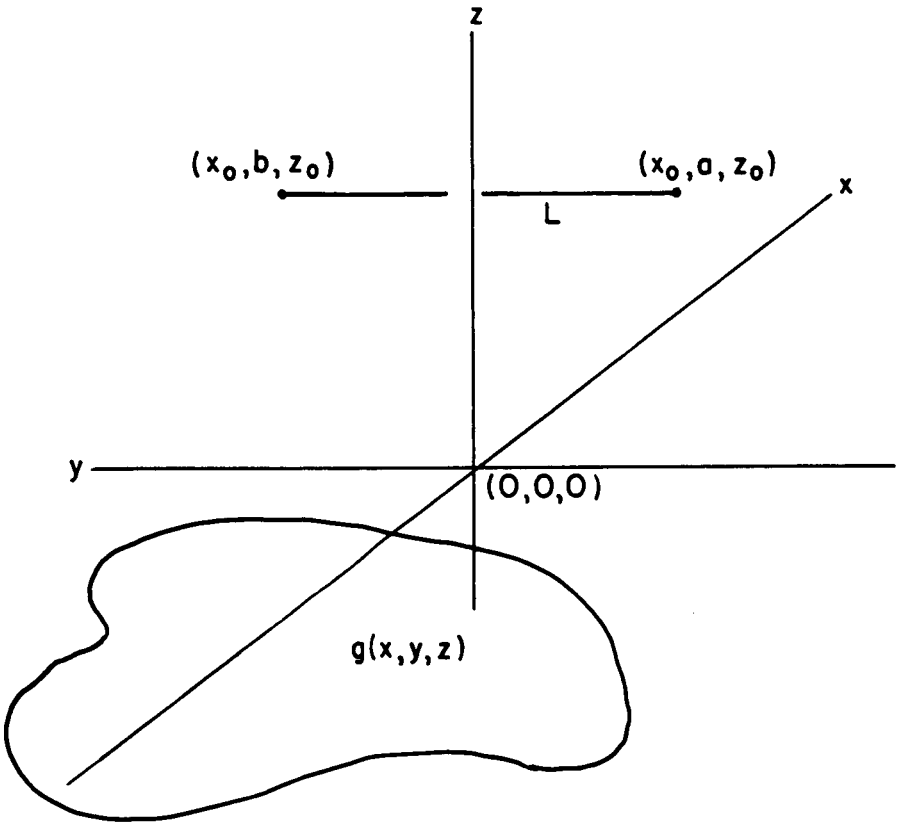

FIG. 1. COORDINATE SYSTEM SHOWING RELATIONSHIP BETWEEN TRAJECTORY AND CURRENT DISTRIBUTIONS.

notation, we may then write the incident wave as

$$e_i = A \exp[j(\omega t - \bar{k}\cdot\bar{r})] , \qquad (1)$$

where $\bar{k}$ is the wave vector $|\bar{k}| = 2\pi/\lambda$, $\bar{r}$ is the position vector, and λ is the free-space wavelength of the incident radiation. Let $g(x, y, z)$ be a vector component of the current distribution on the surface of B resulting from e_i. From electromagnetic theory e_s is then

$$e_s = \exp[j\omega t] \int_{g\neq 0} \frac{g(\bar{r}') \exp[-j|\bar{k}|\,|\bar{r}-\bar{r}'|]}{|\bar{r}-\bar{r}'|}\, dv' ,$$

or, if $p = \exp[-j\bar{k}\cdot\bar{r}]/|\bar{r}|$, then $e_s = g*p \exp[j\omega t]$, where $*$ denotes convolution. It is tempting to consider $g(\bar{r})$ as a current sheet and to write the expression for e_s as an integral over ds rather than over dv. However, the optical depth of a radar signal impinging on a planetary surface may be a considerable number of wavelengths, and the scattered fields must be written in terms of volume elements even though the currents have a two-dimensional character.

The incident and reflected waves form an interference pattern in the space above the surface of B with a time average power (in the case of noiseless square-law detection) of

$$P = (e_s+e_i)\ (e_s+e_i)^* = |e_s|^2 + |e_i|^2 + e_s e_i^* + e_s^* e_i \ ,$$

where * indicates the complex conjugate. Substituting for e_i from Eq. (1), we have

$$P(x,y,z) = |A|^2 + |e_s|^2 + A^* e_s \exp[-j\bar{k}\cdot\bar{r}] + A e_s^* \exp[j\bar{k}\cdot\bar{r}] \ .$$

Since the $\exp[j\omega t]$ is lost in detection, e_s now refers to the spatial variation of the fields. If $\xi = \cos(\bar{k},L)$, then along L the power

$$P(x,y,z) = |A|^2 + |e_s|^2 + A^* e_s(x_0,y,z_0) \exp[-j(2\pi/\lambda)\xi y]$$

$$+ A e_s^*(x_0,y,z_0) \exp[j(2\pi/\lambda)\xi y] \ . \quad (2)$$

The spatial Fourier spectrum along L is

$$F(P) = S(u) = |A|^2\ \delta(u) + E_s * E_s^* + A^* E_s(u + \frac{2\pi}{\lambda}\xi) + A E_s^*(-u + \frac{2\pi}{\lambda}\ \xi) \ ,$$

where upper-case letters represent the Fourier transform with respect to y of the corresponding lower-case symbols. The squaring operation produces a constant $|A|^2$, some intermodulation products $|e_s|^2$ centered

on the spatial frequency axis, and a spatial carrier $\cos[(2\pi/\lambda)\xi]$, modulated by e_s. Clearly, if u_{max} is the greatest frequency in e_s, and if $(2\pi/\lambda)\xi$ is greater than $3u_{max}$, then e_s may be recovered from the power by a filtering operation. The output spectrum of the detector is illustrated in Fig. 2; this is a result that is well known in holography [Ref. 2].

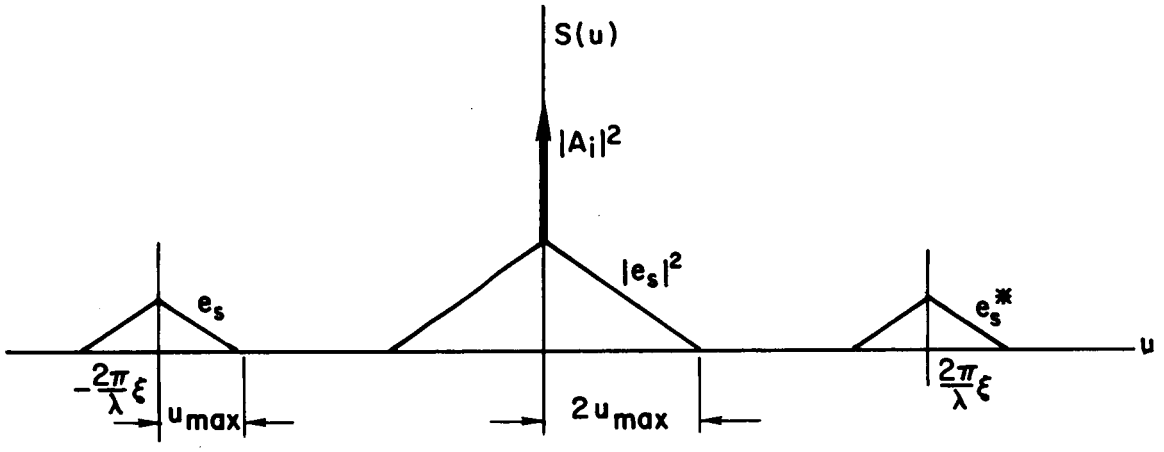

FIG. 2. SPATIAL FREQUENCY DISTRIBUTION OF DIRECT AND REFLECTED SIGNALS.

Although square-law detection has been discussed here because it is a simple way to recover the scattered field and because it makes the analogy with holography more vivid, it is not essential to the process. In bistatic-radar mapping there are other detection schemes that may be used to some advantage.

The salient feature of this development thus far is that the system is self-calibrating. One may think of the incident wave as providing a reference signal with which the scattered wave is compared and which allows both the amplitude and phase of the scattered fields to be recovered, with the exception of an unimportant phase factor. Physically, the surfaces of constant phase difference between the incident wave and the fields scattered by a point are paraboloids in space. Consequently the interference pattern of a single scatterer and a plane wave is a family of paraboloids of maxima and minima of power. The relative positions and

amplitudes of the families of paraboloids associated with different targets reveal the relative position and amplitudes respectively of the targets themselves. The scattered field which is a linear superposition of the patterns of the many scatterers that make up the surface, is preserved in the cross terms of the detection process. In effect, a spacecraft sampling the power along L is sampling these patterns and it is in this way that a space vehicle can provide information about the scattered wavefronts along its trajectory.

If e_s is convolved with p^*, the result is

$$g' = e_s * p^* = g * p * p^*$$

$$g'(r) = \int_a^b \frac{\exp\left\{-j|\bar{k}|\left[(x-x_0)^2+(y-y'')^2+(z-z_0)^2\right]^{1/2}\right\}}{\left[(x-x_0)^2+(y-y'')^2+(z-z_0)^2\right]^{1/2}} \cdot \int_{g\neq 0} \frac{g(x',y',z')\,\exp\left[j|\bar{k}|(x_0-x')^2+(y''-y')^2+(z_0-z')^2\right]^{1/2}}{\left[(x_0-x')^2+(y''-y')^2+(z_0-z')^2\right]^{1/2}}\, dv'dy'' .$$

For g' corresponding to a point target T at (x_1,y_1,z_1), we have

$$g'_\delta(\bar{r}) = \int_a^b \frac{\exp\left[j|\bar{k}|\left\{\left[(x_0-x_1)^2+(y''-y_1)^2+(z_0-z_1)^2\right]^{1/2} - \left[(x-x_0)^2+(y-y'')^2+(z-z_0)^2\right]^{1/2}\right\}\right]}{\left[(x_0-x_1)^2+(y''-y_1)^2+(z_0-z_1)^2\right]^{1/2}\left[(x-x_0)^2+(y-y'')^2+(z-z_0)^2\right]^{1/2}}\, dy'' .$$

Some simplification results from letting $r_0^2 = (x_1-x_0)^2+(z_1-z_0)^2$ and $(r_0-\Delta r)^2 = (x_0-x)^2+(z_0-z)^2$, so that

$$g'_\delta(\Delta r,y) = \int_a^b \frac{\exp\left[j|\bar{k}|\left\{\left[r_0^2+(y''-y_1)^2\right]^{1/2} - \left[(r_0-\Delta r)^2+(y-y'')^2\right]^{1/2}\right\}\right]}{\left[r_0^2+(y''-y_1)^2\right]^{1/2}\left[(r_0-\Delta r)^2+(y-y'')^2\right]^{1/2}}\, dy'' ,$$

(3)

where r_0 is clearly the distance from L to a parallel line containing the target, Δr is the distance from the target projected onto the plane containing T and L, measured positively toward L, and (y_1-y) is distance from T in the y direction. No generality is lost if we take $y_1 = 0$. Normalizing so that $g'_\delta(0,0) = 1$,

$$g'_\delta(\Delta r, y) = \frac{r_0}{\tan^{-1}(x/r_0)\Big|_a^b} \int_a^b \frac{\exp\left[j|\bar{k}|\left\{[r_0^2+y''^2]^{1/2} - [(r_0-\Delta r)^2+(y-y'')^2]^{1/2}\right\}\right]}{[r_0^2+y''^2]^{1/2}\,[(r_0-\Delta r)^2+(y-y'')^2]^{1/2}}\, dy'' . \quad (4)$$

With $\Delta r = 0$, Eq. (4) is the voltage antenna pattern of a uniformly illuminated, perfectly corrected, coherent, side-looking radar focused at range r_0 [Ref. 3]. However, from the form of Eq. (4) it is clear that the amplitude of the pattern falls off with Δr as well as with y. It is this fact that makes possible the resolution in range without the use of pulsed waveforms.

In addition, Eq. (4) will be recognized as the matched-filter response to a (spatial) signal $p(\bar{r})$. It is also the equation of the image of a point formed through a slit. Equation (4), together with the method for separating e_s from e_i, is a direct analogue of a one-dimensional hologram. These relationships will be used later to provide better understanding of the processing involved in the image formation.

Taking the usual radar condition that separate targets have a uniform phase distribution (so that power superposition holds for the statistically expected response) allows the power pattern $I(\Delta r, y) = |g'_\delta|^2$ to be viewed in the same manner that Woodward's ambiguity function [Ref. 4] is in determining resolution in pulsed radar. The difference lies in that $I(\Delta r, y)$ gives resolution in range and lateral displacement while the ambiguity function describes a system's response in range and range rate. (Note that Eq. (4) is not equivalent to the ambiguity function, only similar.) Loosely speaking, where $I(\Delta r, y)$ resulting from some target is large compared to the peak signal from a second target, the second target will be obscured. In this way $I(\Delta r, y)$ indicates fundamental system limitations on the resolution that may be achieved.

If one measures all distances in wavelengths and assumes $(b-a)/2r_0 < 0.1$, then $I(\Delta r, y)$ may be approximated by

$$I(\Delta r,y) = \frac{r_0(r_0-\Delta r)}{2\Delta r(b-a)^2}\left[\left\{C\left(x\left[\frac{2\Delta r}{r_0(r_0-\Delta r)}\right]^{1/2} - y\left[\frac{2r_0}{\Delta r(r_0-\Delta r)}\right]^{1/2}\right)\Bigg|_{x=a}^{x=b}\right\}^2 + \left\{S\left(x\left[\frac{2\Delta r}{r_0(r_0-\Delta r)}\right]^{1/2} - y\left[\frac{2r_0}{\Delta r(r_0-\Delta r)}\right]^{1/2}\right)\Bigg|_{x=a}^{x=b}\right\}^2\right], \qquad (5)$$

where C and S represent the Fresnel integrals for cosine and sine respectively. As $\Delta r \to 0$ it can be shown that Eq. (5) becomes

$$I(\Delta r,y)_{\Delta r\to 0} = \operatorname{sinc}^2\left[y\,\frac{b-a}{r_0}\right]. \qquad (6)$$

Typical contours of Eqs. (5) and (6) are given in Fig. 3. Note that all dimensions are in wavelengths. The one-half-power resolution in Δr and

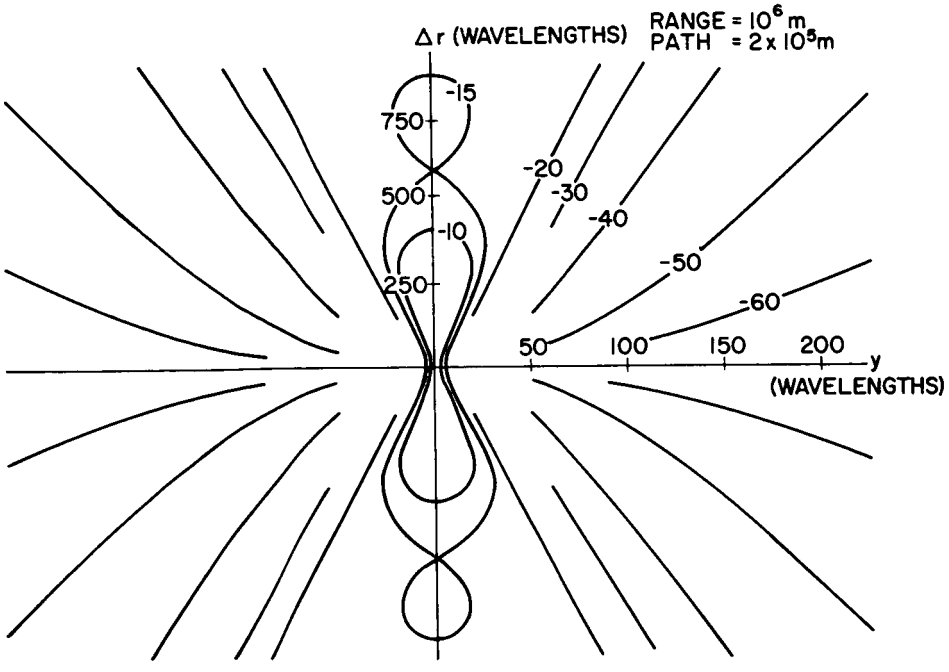

FIG. 3. ISOPHOTES OF RESPONSE TO A POINT SOURCE. Contours are in decibels.

y, still measured in wavelengths, may be shown to depend only on $f = (b-a)/r_0$. Along y the resolution is proportional to the reciprocal of f, along Δr, to the inverse square of f.

It should be clear that $I(\Delta r, y)$ is a figure of revolution about L and that Δr refers only to changes in range. Thus, when the current distribution g lies entirely in a plane containing L, $I(\Delta r, y)$ gives the resolution. If g lies in some other plane, then $I(\Delta r, y)$ must be modified by replacing Δr by $\Delta r' \cos \theta$, where $\Delta r'$ is the distance normal to y measured in the plane containing g, and θ is the apparent angle included between a line to L and the plane containing g. This relationship also holds for conventional side-looking radar.

If Fig. 4 is extrapolated to higher f's, it seems reasonable to expect the resolution to continue to improve, at least until f = 1; there are good physical arguments indicating that higher resolutions can be obtained. It is certainly clear that, for sufficiently short wavelengths,

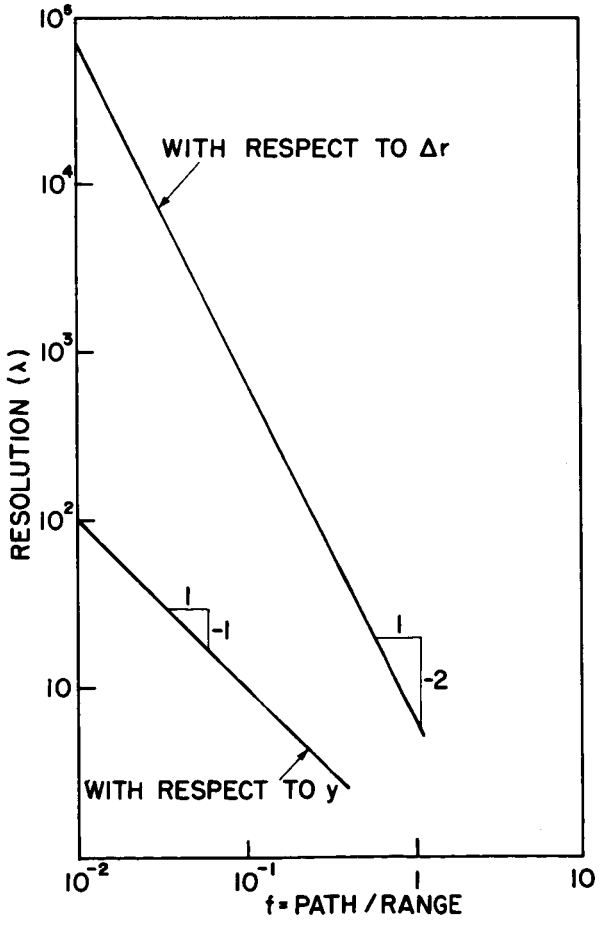

FIG. 4. RESOLUTION VS SYSTEM f NUMBER. $f = (b-a)/r_0$.

the distance $D/2$ often quoted as the maximum resolution transverse to the flight path of a side-looking radar can be exceeded for any f.* Actually, there is no problem, since $D/2$ is a practical rather than the fundamental limit, growing out of the practice of employing antennas of fixed orientation on aircraft. The results quoted in this paper can be achieved even with narrowbeam antennas if the area to be mapped is restricted so that it can always be viewed from the flight path and the antenna is continually aimed at this area as the radar carrier goes by; that is, one may trade resolution for the size of the area to be mapped and vice versa.

When radars employing pulsed waveforms are utilized for mapping, it is easy to visualize how resolution in range and azimuth are obtained. Just how this works when continuous waveforms are employed may not be quite so obvious. It can be explained by an optical analogy.

It is elementary in optics that the resolution transverse to the optic axis of an imaging system depends on the size of the system aperture in wavelengths. In addition, there exists in a focused image a longitudinal resolution associated with the focusing itself [Ref. 6].

For a two-dimensional aperture, the definition of the image along the optic axis depends on the focal length of the system and the aperture size. Thus an imaging system employing a two-dimensional aperture actually re-creates a three-dimensional image. Focusing a camera corresponds to placing the image of the subject on the film plane. If a lens is made to image through a one-dimensional aperture by placing a slit just behind the lens, resolution is completely lost in the direction orthogonal to the plane formed by the slit and the optic axis and degraded somewhat in the other two directions. It is easy to show that the image has been integrated in the direction transverse to the slit. For a discussion on one-dimensional apertures, see Bracewell [Ref. 7]. For the special case of a planar object parallel to the slit, very little is lost, since the brightness distribution of the image in the plane corresponding to the object is essentially preserved.

*D is the size of the effective aperture of the radar antenna. [Ref. 5].

Figure 5 represents the imaging of two point sources with a two-dimensional aperture. Figure 6 shows how the image of the same two point sources might look if the aperture were blocked in one dimension. Smearing of the image occurs transverse to the slit but resolution is otherwise maintained.

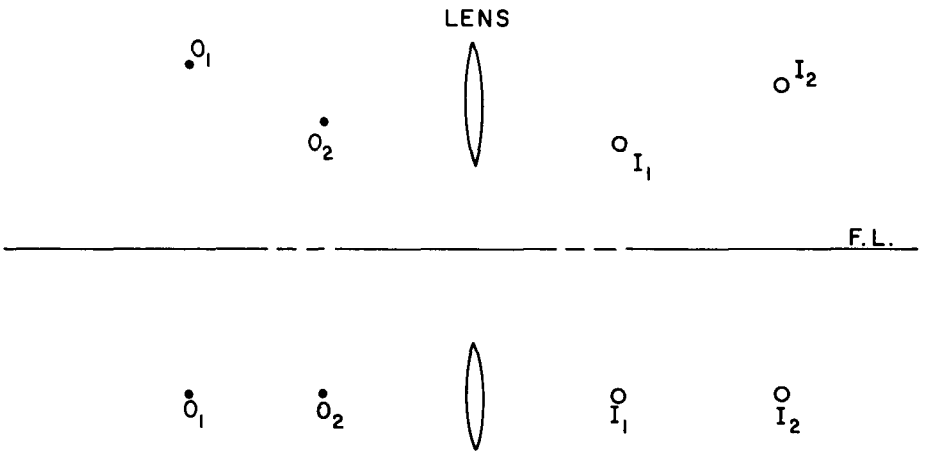

FIG. 5. IMAGING WITH A TWO-DIMENSIONAL APERTURE.

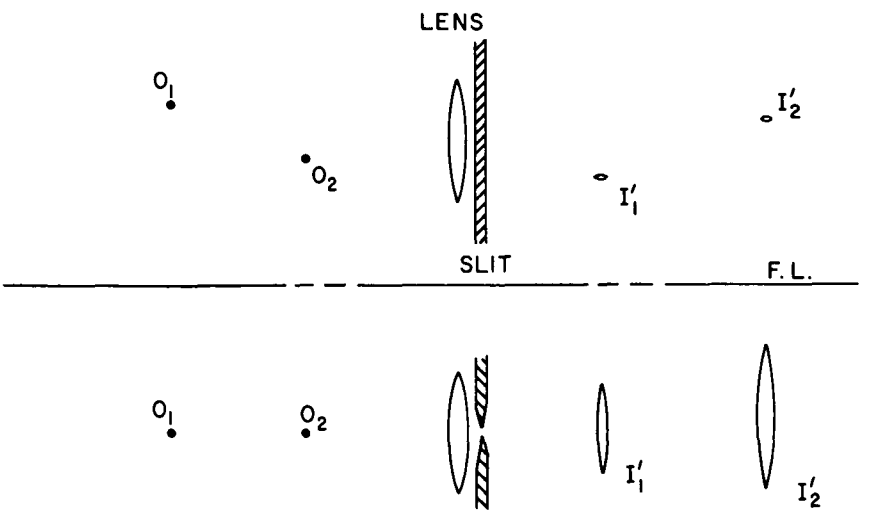

FIG. 6. IMAGING WITH A ONE-DIMENSIONAL APERTURE.

The hologram provides a photographic analogue of bistatic radar. When illuminated with a fan-shaped beam of monochromatic light, the real image produced is equivalent to the image produced by a slit-covered lens; the entire process of making the hologram and playing it back with a fan-shaped beam corresponds to the bistatic-radar mapping scheme described in this paper.

Encouraging preliminary experimental results in support of bistatic radar have been obtained by exploiting this analogy. Figure 7 shows an ordinary photograph of some washers on a black background. Figure 8 is the real image of the hologram of this object. Figure 9 is the real image of the hologram of the object when the hologram was illuminated with coherent light from a 20-micron slit, 2 cm long placed just behind the hologram. The wavelength was 0.6328 microns from an He-Ne laser. The mean distance from the slit to the image was about 12 cm. In both Figs. 8 and 9 the image is recorded in the plane that was occupied by the object when the hologram was taken. Figures 8 and 9 are oriented so that the slit would be at the bottom of the pictures. The vertical smear on Fig. 9 is the diffraction pattern of the slit. Some aberrations were introduced in Figs. 8 and 9 by the experimental difficulties associated with intensely illuminating a narrow slit. Therefore, Fig. 9 should be compared with Fig. 8 only to see the effects of the slit and should not be taken as representing fundamental limits on resolution.

Figure 9 does have precisely the characteristics predicted by Figs. 3 and 4--two-dimensional resolution and better resolution in the plane transverse to the slit than perpendicular to it. Obviously, the general nature of the washers can still be determined.

The only difference between bistatic-radar mapping and the hologram is that in the hologram the fields along L are measured simultaneously while in the radar case the fields are measured sequentually in time. Flying a vehicle along L merely introduces a linear-scale change from the space-frequency domain to the time-frequency domain in the output of the detector.

Even though the discussion to this point has dealt with stationary objects, perfectly coherent illumination, and linear trajectories, it appears feasible to apply the mapping technique to the Moon and the planets.

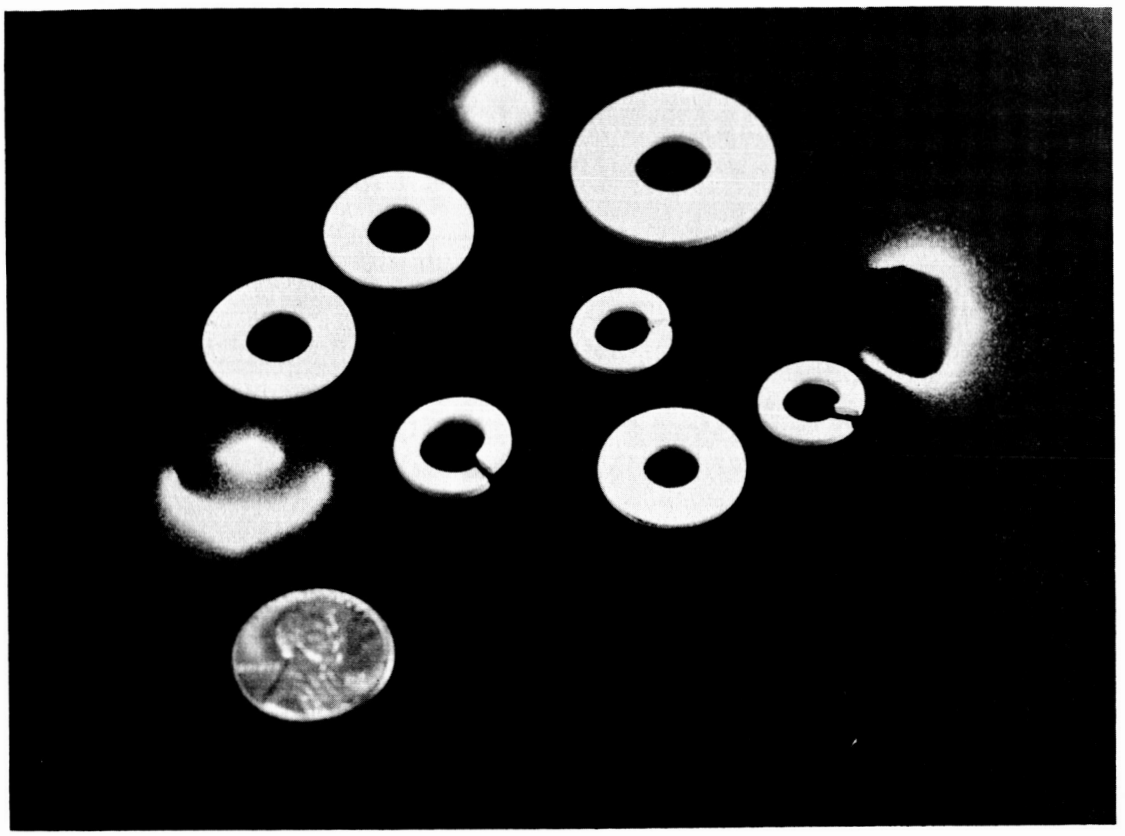

FIG. 7. TEST OBJECT FOR HOLOGRAM ANALOGY.

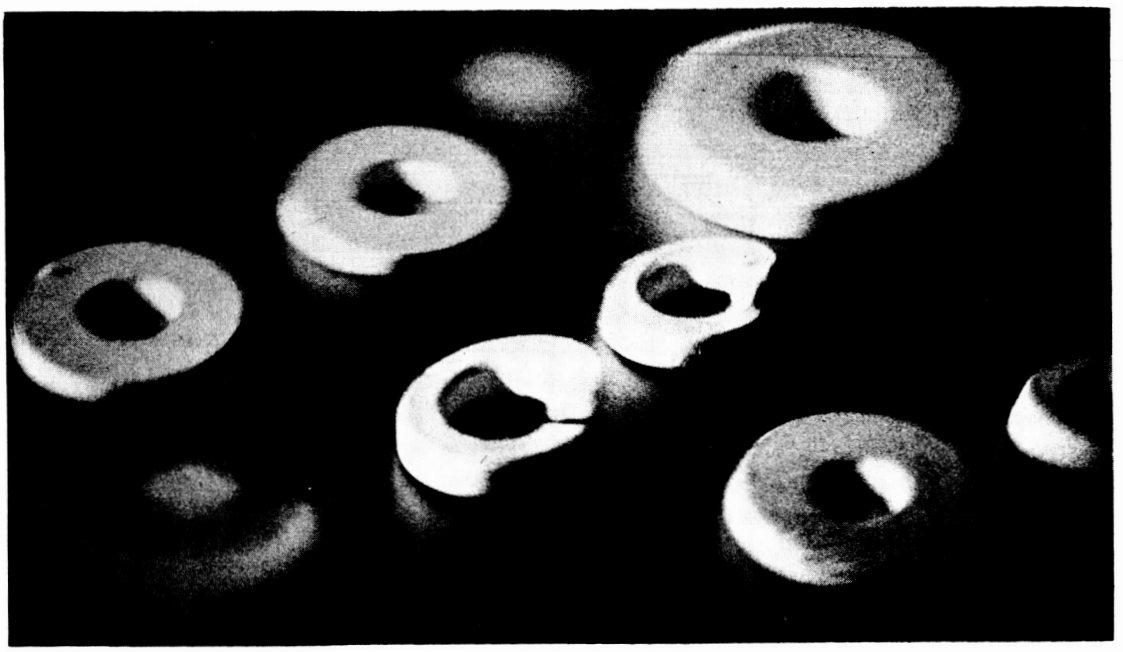

FIG. 8. REAL IMAGE OF HOLOGRAM.

FIG. 9. REAL IMAGE OF HOLOGRAM THROUGH 20-MICRON SLIT, 2 cm LONG.

Allowing the trajectory to curve amounts to making ξ, the direction cosine between the incident wave and the path, a function of distance along the path. For $\xi(y)$ slowly varying with respect to e_s, the previous results hold. Once it is realized that the entire imaging system depends primarily on removing the phase introduced by the scattering process there is no difficulty understanding the correction for $\xi = \xi(y)$. [c.f. Eq. (4)].

A planet rotates very slowly compared to the orbit times currently envisioned for planetary studies. Consequently, during the time required for an orbiter to inspect some region of interest the planet moves only slightly (linear motion is of no importance) so that the principal effect on e_s will be a shift in its spatial orientation. To a vehicle passing through the interference pattern this appears as a change in the velocity of the spacecraft relative to the pattern and can be removed from the data. An alternate, perhaps more direct, point of view is that rotation introduces a perturbation in the phase path from a point on the planet to a point in the orbit with respect to the phase path for a stationary

body, but it is a perturbation that can be calculated and accounted for in the imaging process.

The effect of finite spectral width enters in the form of the autocorrelation function of the illuminating wave as an amplitude-weighting factor in Eq. (4), with an argument of the total time delay between e_i and e_s. Thus, if the coherence length of the illuminating wave train is greater than the path difference between e_i and e_s, Eq. (4) stands. The coherence length of the transmitted wave can be truly enormous. However, the randomizing effects of the interplanetary medium and planetary atmospheres must be accounted for. Current data suggest that radio frequencies above 200 or 300 Mc will be usable over an astronomical unit.

Since Eq. (4) represents a matched-filter response (correlation detection) it is optimum in the sense that the signal-to-noise ratio for a given target is maximized. A well-known property of such filters is that, for a white-noise process, the output signal-to-noise ratio is expressed by

$$\left(\frac{S}{N}\right)_{out} = \frac{2E}{N_0}$$

where E is the total energy in the signal and N_0 is the spectral density of the noise [Ref. 8]. Assuming a receiver noise temperature of several hundred degrees, an input transmitter power of 1 Mw, a total antenna gain of 65 db, and an integration time of 100 sec at a range of 1000 km, objects with a bistatic-radar cross section of 10,000 m^2 should have a signal-to-noise ratio of unity over a distance of 1 A.U. This corresponds to the specular reflection from a projected patch of ground on the order of 300 m on a side.

Until now, the model has been developed in terms of illuminating a planet and receiving the scattered fields on board an orbiter. While perhaps more difficult to conceptualize, the reciprocity theorem assures us (and it can be shown directly) that the same results hold for transmissions from the orbiter to the Earth. Consequently, when the signal-to-noise ratio for the reflected ray is sufficiently high, as it may be

in the case of lunar orbiters, the down-link signal--e.g., the telemetry carrier from an orbiter--may also be used for mapping. Ground-based transmitters will evidently be required for planetary ranges.

A great deal more work, both experimental and theoretical, is obviously required before the experiment described in this paper can be implemented. However, we believe that we have demonstrated the basic scientific soundness and technical feasibility of radar mapping in a bistatic continuous-wave mode.

REFERENCES

1. D. Gabor, "A New Microscope Principle," Nature, 161, 1948, p. 777.
2. E. N. Leith and J. Upatnieks, "Reconstructed Wavefronts and Communication Theory," J. Opt. Soc. Am., 52, 10, Oct 1962, pp. 1123-1130.
3. H. L. McCord, "The Equivalence among Three Approaches to Deriving Synthetic Array Patterns and Analyzing Processing Techniques," IRE Trans. on Mil. Electronics, MIL-6, Apr 1962, pp. 116-119.
4. P. M. Woodward, Probability and Information Theory with Application to Radar, McGraw-Hill Book Co., New York, 1953.
5. L. J. Cutrona and G. O. Hall, "A Comparison of Techniques for Achieving Fine Azimuth Resolution," IRE Trans. on Mil. Electronics, MIL-6, Apr 1962, pp. 119-121.
6. M. Born and E. Wolf, Principles of Optics, Pergamon Press, New York, 1959, pp. 438-448 (especially p. 439).
7. R. N. Bracewell, "Radio Astronomy Techniques," Handbuch der Physik, ed. by S. Flügge, Springer-Verlag, Berlin, vol 54, 1963.
8. George L. Turin, "An Introduction to Matched Filters," IRE Trans. on Information Theory, IT-6, Jun 1960, pp. 311-329.